PNAS
www.pnas.org

Supplementary Information for

Anatomy of a Selectively Co-assembled β-sheet Peptide Nanofiber

Authors: Qing Shao[a,1], Kong, M. Wong[b,1], Dillon T. Seroski[c,1], Yiming Wang[a], Renjie Liu[c], Anant K. Paravastu[b], Gregory A. Hudalla[c], Carol K. Hall[a,*]

Author Affiliations:
[a]Department of Chemical and Biomolecular Engineering, North Carolina State University, Raleigh, NC 27695, USA
[b]School of Chemical and Biomolecular Engineering, Georgia Institute of Technology, Atlanta, GA, 30332, USA
[c]J. Crayton Pruitt Family Department of Biomedical Engineering, University of Florida, Gainesville, FL 32611, USA

[1] Q.S., K.M.W., and D.T.S. contributed equally to this work

*** Corresponding author: Carol K. Hall**
Email: hall@ncsu.edu

This PDF file includes:

www.pnas.org/cgi/doi/10.1073/pnas.1912810117

Supplementary Information Text

Materials and Methods

DMD simulations

Discontinuous Molecular Dynamics (DMD) simulations are used to investigate spontaneous aggregation of complementary charged peptides. For DMD simulations with both CATCH(+) and CATCH(-) peptide chains, the initial configuration was prepared by randomly placing 48 CATCH(+) and 48 CATCH(-) peptide chains in a 200.0×200.0×200.0 nm^3 box (20 mM). For DMD simulations with only CATCH(+) or CATCH(-) peptides, 96 peptide chains were placed in the simulation box with a concentration of 20 mM. The PRIME20 model developed in the Hall group was used to describe the peptide-peptide interactions[1]. Each amino acid residue is modeled using four interactive sites: three backbone spheres C_α, NH, CO and one sidechain sphere. PRIME20 has unique geometric and energetic parameters for each of the 20 different amino acids. Specifically, each sidechain sphere of the 20 amino acids has a distinct hard sphere diameter (effective van der Waals radius), and distinct sidechain-to-backbone distances (R-Cα, R-NH, R-CO). The potential energy function between two amino acid sidechain beads is modeled as a square well potential; the energy parameters between the 20 different amino acids (except for glycine) include 210 independent square well widths and 19 independent square well depths. Backbone hydrogen bonding interactions are modeled as a directional square well potential. The detailed description of the derivation of the PRIME20 geometric and energetic parameters along with their values are given in our earlier work[2-4]. Previous research has affirmed the ability of the PRIME20 model to predict and describe the aggregated structures of peptides. DMD/PRIME20 has been applied to short peptide systems including $A\beta_{16\text{-}22}$[5], palindromic fragments of the prion proteins[6], the designed hexapeptide sequences of Lopez de la Paz *et al.*[7-8], and the tau fragment[9], as well as longer peptide systems including $A\beta_{17\text{-}36}$[10], $A\beta_{17\text{-}42}$[11], $A\beta_{1\text{-}40}$[12], myocilin fragments[13], and prion protein fragments $PrP_{120\text{-}144}$[14-15].

Canonical-ensemble (NVT ensemble) DMD simulations were conducted using our in-house code. DMD is an alternative to classical MD simulations. Instead of solving Newton's equation of motion at regularly spaced time steps, DMD simulations proceed by solving the dynamics after each event between any two interacting sites. The temperature of the simulation system was controlled at T^*=0.20 using the Andersen thermostat and is equivalent to temperature (342 K) with the PRIME20 model[14]. Ten independent DMD simulations were conducted for each system; and each DMD simulation contains 500 billion collisions, equivalent to 16 μs[14]. The criteria for determining when pairs of peptides adjacent to each other are in a β-barrel or a β-sheet are the following. Any two peptide chains are considered to form a pair if they form >5 hydrogen bonds between them. Two peptides are in the same cluster if they form either >5 hydrogen bonds or >1 hydrophobic association. The tail and head amino acid resides are excluded from either calculation.

Experiment

Peptide Synthesis and Purification

Peptides were synthesized using standard Fmoc solid-phase peptide synthesis on a CS336X automated peptide synthesizer (CS Bio) using standard amino acids or a ^{13}C-enriched phenylalanine at position six. Peptides were acetylated at their N-termini using 10% acetic anhydride (Sigma), 80% dimethylformamide (Fisher), and 10% *N*,*N*-Diisopropylethylamine (Fisher). Synthesized peptides were then collected and washed 10 times with acetone and placed in vacuo overnight. Peptide deprotection and cleavage from resin was done using 95% trifluoracetic acid (TFA) (Fisher Scientific), 2.5% triisopropylsilane (Sigma-Aldrich), and 2.5% ultrapure water. Soluble peptide was separated from the solid resin using disposable polypropylene columns with 0.2 μM filters and then precipitated using diethyl ether (Fisher Scientific) on ice for 5 minutes. The precipitate was then pelleted *via* centrifugation and washed with fresh diethyl ether three times to remove residual TFA, and then dried in vacuo overnight. Peptides were either dissolved in water

[CATCH(+)] or 200 mM ammonium bicarbonate [CATCH(-)], frozen, and freeze-dried with a FreeZone 1 lyophilizer (Labconco).

Peptides were purified to greater than 90% purity using reverse phase high-performance liquid chromatography (RP-HPLC) on a DionexTM Ultimate 3000TM System (Thermo Scientific) equipped with a C-18 column (Thermo Scientific) for CATCH(6-), or a PFP column (Thermo Scientific) for CATCH(4+) (Fig. S17A). The mobile phase consisted of (A) water with 0.1% TFA and (B) acetonitrile with 0.1% TFA. Peptides were detected by absorbance at 215 nm. Molecular weights were verified using matrix assisted laser desorption/ionization time-of-flight (MALDI-TOF) mass spectrometry by mixing 1:1 with 10 mg/ml α-Cyano-4-hydroxycinnamic acid matrix in 30% water, 70% acetonitrile, and 0.1% TFA (Fig. S17B).

Nanofiber preparation and formation

Peptides were dissolved either in water [CATCH(4+)] or 200 mM ammonium bicarbonate [CATCH(6-)] with their concentrations determined using phenylalanine absorbance (λ = 258 nm). Unless otherwise stated, all two-peptide component samples contain an equimolar ratio of peptides which are then infused with 10x phosphate-buffered saline (PBS) (137 mM NaCl, 2.7 mM KCL, 10 mM Na_2HPO_4 and 1.8 mM KH_2PO_4, pH 7.4) to reach the desired final concentration in 1x PBS. Single component peptides are dissolved and infused with 10x PBS to reach 1x PBS at the desired concentration.

Fourier Transform Infrared Spectroscopy (FTIR)

The FTIR spectra were recorded on a Frontier FTIR spectrophotometer (PerkinElmer) equipped with a universal ATR sampling accessory. For aqueous samples, the FTIR spectrophotometer was blanked with ultrapure water prior to scanning. Samples were prepared at 10 mM and 1x PBS with 5 µl spotted onto the ATR accessory. Aqueous samples were scanned 50 times with the average of the spectra reported. Dry samples were spotted and dried on the ATR accessory and then scanned 4 times with the average of the spectra reported.

Thioflavin T Assay

Peptides were fibrillized in 1x PBS overnight in a 96-well plate (Corning) and then infused with a stock solution containing 0.8 mg/ml Thioflavin T (ThT) (Acros) in water, which was first filtered through a 0.22 µm syringe filter (Millex). Final ThT concentration in peptide samples was 0.08 mg/ml. Samples were analyzed using a SpectraMax M3 spectrophotometer (Molecular Devices) using excitation 450 nm and emission 482 nm. All samples were run in triplicate, with the mean and standard deviation reported.

Solid-state NMR

Peptide hydrogels were prepared at 10 mM in 1x PBS and then statically incubated for 24 hours. Nanofibers were sedimented via centrifugation at 12,100 x *g* for 5 minutes and then re-suspended with ultrapure water three times. Samples were freeze-dried, packed into NMR rotors, and minimally hydrated (1 mg of water per mg of peptide). Measurements were performed on an 11.75 T Bruker Avance III spectrometer with a 3.2 mm Bruker MAS probe. ^{1}H-^{13}C CPMAS measurements were run at 20 kHz magic angle spinning (MAS) with 100 kHz proton decoupling and a CP contact time of 2 ms. Reported NMR chemical shifts are relative to tetramethyl silane, as calibrated with adamantane before each experiment. PITHIRDS-CT measurements were conducted at 12.5 kHz MAS using 26.7 µs π-pulses during ^{13}C dipolar recoupling. Total recoupling time was 61.44 ms, where k1 = 4, and k2 + k3 = 16 (terms defined by Tycko[16]). Continuous wave proton decoupling at 100 kHz was applied during the PITHIRDS-CT pulse sequence and data acquisition. Pulsed spin locking was used to improve the sensitivity of our PITHIRDS-CT measurements where indicated[17].

PITHIRDS-CT nuclear spin simulations

To understand the effects of isotopic dilution in the presence of deviation from ideal AB-alternation, we performed Monte Carlo simulations of β-sheets formed by co-assembly of complementary peptides A and B. Each β-sheet pattern is symbolized by a string sequence of A's and B's. The

addition of a peptide to the end of a β-sheet sequence in the Monte Carlo simulations is determined by the identity of the current peptide at the end and a probability of AA or BB nearest neighbors. The β-sheet length was set to 2000 peptide units to approximate steady state. Then, the β-sheet sequence patterns were used to create spin simulations to examine dilutions effects on PITHIRDS-CT measurements.

Due to computational limitations of spin simulations, the Monte Carlo predicted β-sheet sequence pattern was sampled in 8-unit long segments at 50 random and distinct locations. Each 8-unit long letter sequence was then mapped to central sites on an ideal antiparallel β-sheet to produce sets of isotopically diluted spin systems. Simulations of PITHIRDS-CT decay curves are then produced using SpinEvolution NMR simulation software on each spin system[18]. The series of simulations are summed across all 50 locations. This procedure was performed 10 times on each Monte Carlo sequence to eliminate sampling artifacts to produce an averaged PITHIRDS-CT decay simulation. Finally, PITHIRDS-CT decays were produced by averaging over 10 Monte Carlo sequences at each simulated percentage of self-association propensity to again reduce sampling bias.

Transmission electron microscopy

To view nanofibers using TEM, peptide solutions in PBS were prepared at specified concentrations and incubation times. Solutions of nanofibers were adsorbed onto Formvar/carbon grids (FCF400-CU-UB, Electron Microscopy Sciences) by placing grids on top of 30 µL sample solution for 30 seconds. Grids were dried by tilting onto a Kimwipe (Kimberly-Clark) and then negatively stained with a 2% aqueous solution of uranyl acetate for 30 seconds and again dried using a Kimwipe. For cold sample preparation, all the procedures were carried out as described above at 4 °C and allowing 5 minutes for grids to fully dry. All samples were viewed using a FEI Tecnai Spirit transmission electron microscope (FEI, The Netherlands) housed in the University of Florida Interdisciplinary Center for Biotechnology Research.

Dynamic Light Scattering

The hydrodynamic diameter of co-assemblies formed in equimolar mixtures of CATCH(+) and CATCH(-) was measured using a NanoBrook 90Plus Particle Size Analyzer and BIC Particle Sizing Software (Brookhaven Instruments). Working solutions of each peptide were filtered through a 0.22 µm filter before size analysis. Samples were then mixed and infused with 10x PBS to reach a final concentration of 1x PBS and read on the DLS at the specified concentrations and time intervals. Hydrodynamic diameters were determined from ten 30 second runs, where 0/100% baseline index runs were removed from the sampling.

Supplemental Data and Figures

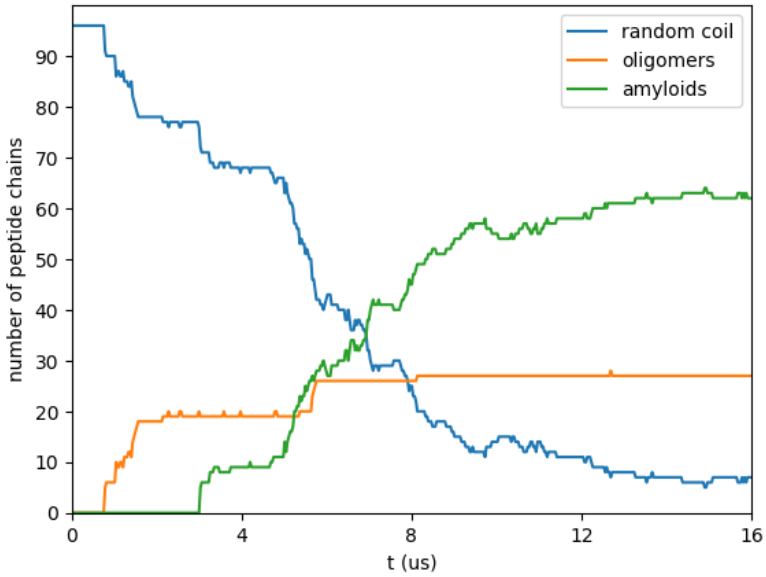

Fig. S1. The numbers of peptide chains in random coil, β-barrel oligomers and amyloid as a function of simulation time. The number of random-coil peptides decreases monotonically as the simulation progresses. The number of peptides in β-barrel oligomers, which first appear at ~1 μs, increases until ~6 μs and remains constant thereafter. The number of peptides in amyloid structures, which first appear at ~3 μs, surpasses that in β-barrel oligomers at around 5 μs, increases rapidly thereafter, and eventually plateaus because the number of peptide chains are fixed in the simulation.

Comparing structural order of on-pathway oligomers and off pathway β-barrel oligomers

The numbers of hydrogen bonds, N_{HB}, in 6- and 7-mer structures along the pathway to amyloid are 5.6 and 5.0, and the numbers of hydrophobic associations, N_{HP}, are 3.1 and 3.8. These numbers are much lower than those for the β-barrel structures shown in Fig. 3E, each of which has 6 to 7 peptides, 7-8 hydrogen bonds and ~5.5 hydrophobic associations. Thus, the oligomers along the amyloid-forming pathway are less structurally ordered than those in the β-barrels; this lack of order serves to create space for additional peptides to join the cluster.

Even-odd asymmetry of perfectly formed β-barrel oligomers affects their ability to grow

There is an interesting asymmetry in the ability of the β-barrels containing even and odd numbers of strands to form mismatches (AA or BB neighbors) and hence to grow by adding strands. This is because β-barrels with an even number of peptides can only have an even number of mismatches (including no mismatch), while those with an odd number of peptides can only have an odd number of mismatches. A consequence of this is that it is advantageous for a β-barrel with an even number of strands to add in a new strand rather than to swap out a matched peptide for a mismatched peptide. This can be seen by estimating the energy of a perfectly formed β-barrel with N_{AB} like neighbors and N_{AA} and N_{BB} unlike neighbors. In this calculation the peptides are assumed to be: (a) antiparallel (since they are palindromes and end-capped in DMD this does not make a difference), and (b) out of register by one amino acid (to capture the slanted alignment of peptides around the β- barrel). We estimated only the electrostatic energy between K and E sidechains and neglected hydrophobic and hydrogen-bonding interactions as these should be relatively independent of the sequence. The energy for (a cylindrical arrangement) of peptides with N_{AB} like neighbors and N_{AA} and N_{BB} unlike neighbors is $N_{KE}(8\varepsilon_{KE}) + N_{KK}(7\varepsilon_{KK}) + N_{EE}(9\varepsilon_{EE})$, where ε_{ij} is the electrostatic interaction between amino acids of types i = E or K. Of the β-barrel peptides that we saw, 6-mers and 7-mers, their electrostatic energy follows the order: E(perfect 6-mer) < E(7-mer with 1 mismatch) < E(6-mer with 2 mismatches) < E(7-mer with 3 mismatches). Thus to

accommodate a mismatch, it is energetically favorable for the β-barrel to grow bigger rather than to substitute in a new necessarily mismatched peptide. The real scenarios are more complicated due to the contribution of backbone hydrogen bonding, dihedral angle constraints and hydrophobic associations between F-F sidechains.

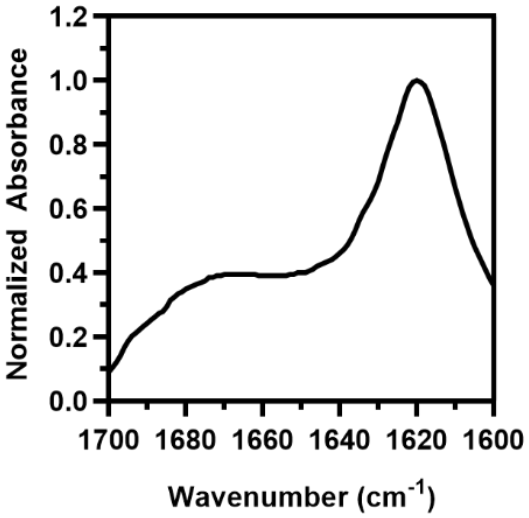

Fig. S2. FTIR spectra of aqueous 10 mM CATCH(+/-) in 1x PBS demonstrating a β-sheet maximum at 1620 cm^{-1}.

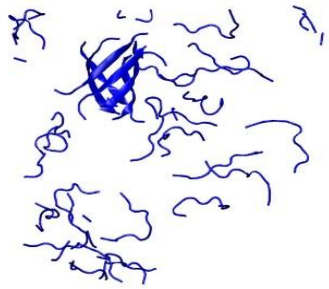	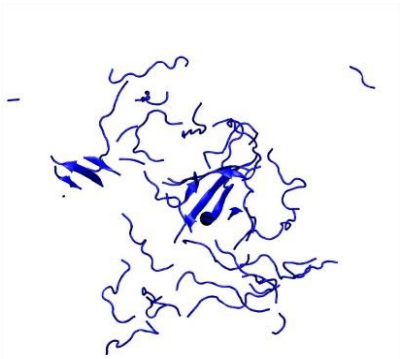
CATCH(+)	CATCH(+)

Fig. S3. Two snapshots that demonstrate transient self-assembly of CATCH(+) peptides during DMD simulations.

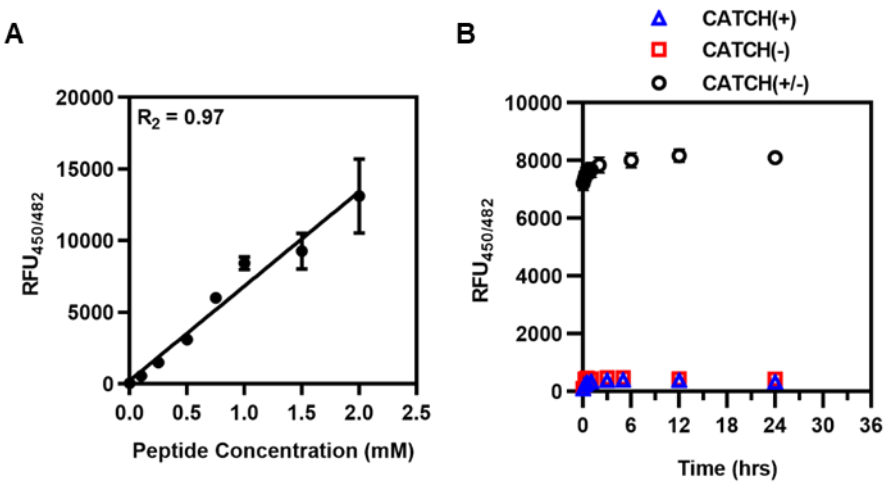

Fig. S4. (A) Standard curve relating equimolar CATCH(+/-) peptide concentration to Thioflavin T fluorescence demonstrating linearity of RFU signal with peptide concentration. (B) ThT kinetics of 1 mM peptide alone or mixed. Key: (CATCH(+), blue triangle; CATCH(-), red square; CATCH(+/-), black circle).

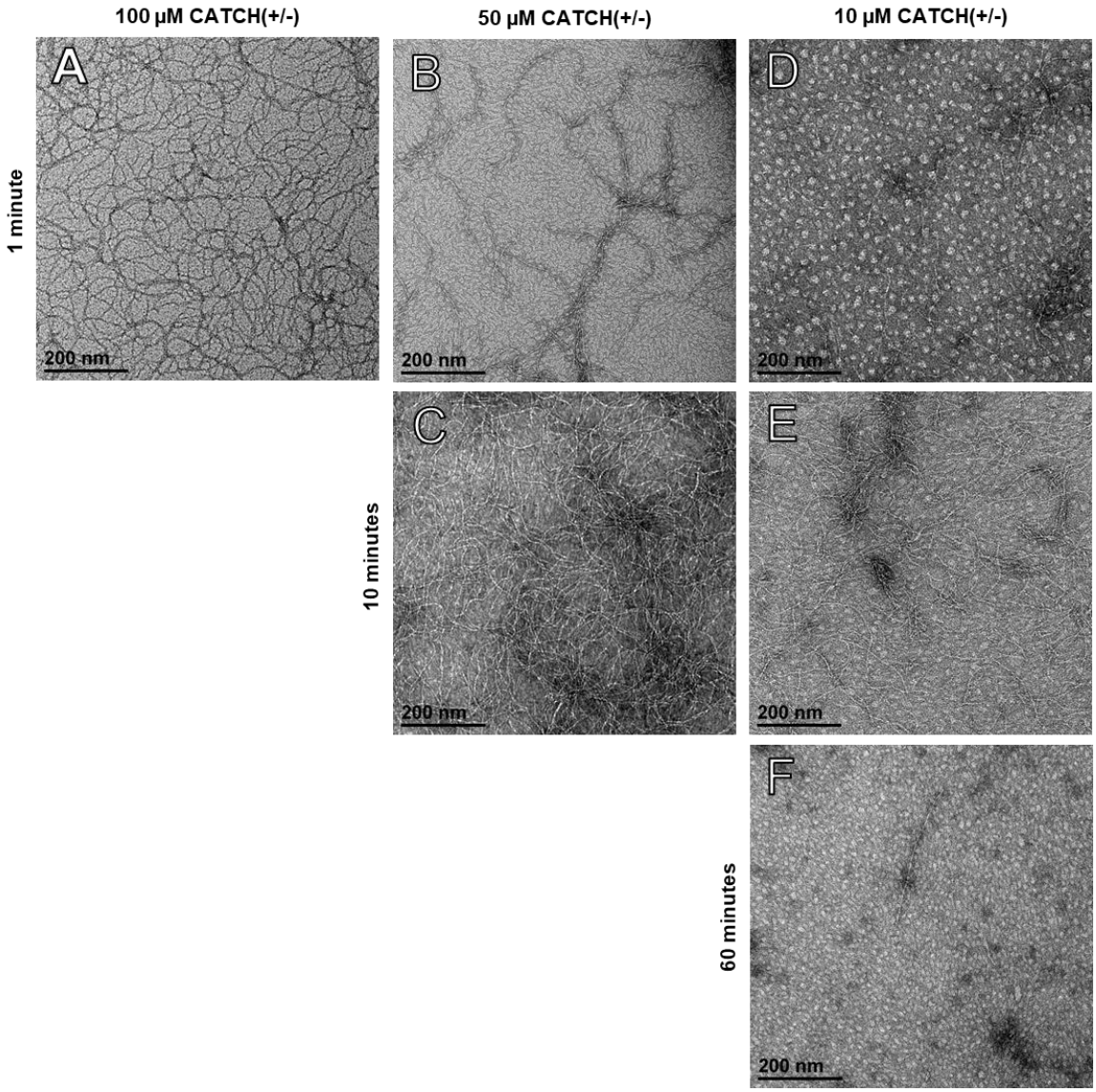

Fig. S5. Full-size electron micrographs of 100 (left column), 50 (center column), and 10 µM (right column) CATCH(+/-) at 1 min (top row), 10 minutes, (middle row), and 60 minutes (bottom row) from Fig. 4B-C.

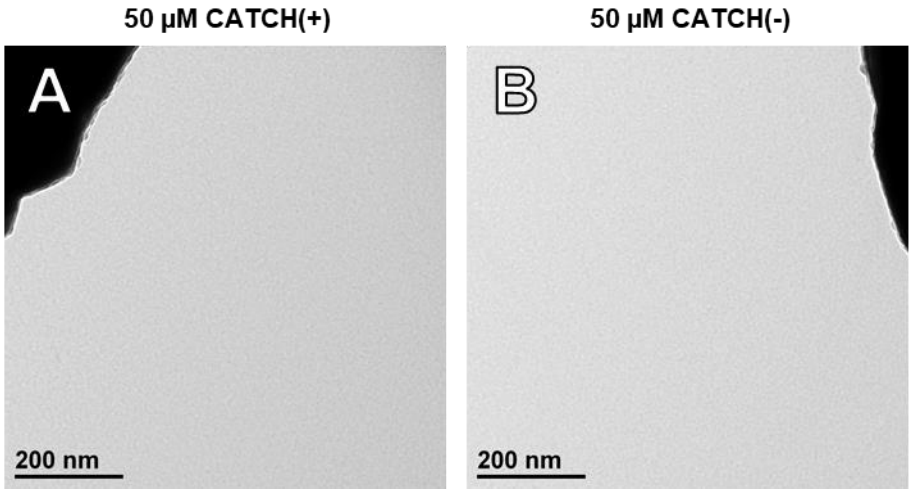

Fig. S6. Full-size electron micrographs of 50 µM (A) CATCH(+) or (B) CATCH(-).

CATCH(+/-) TEM prepared under cold (4 °C) conditions

A combination of round particles and elongated nanofibers were observed in samples of 100 μM CATCH(+/-) maintained for 1 minute at 4°C (Fig. S7A). In 50 μM CATCH(+/-) samples at 4°C (Fig. S7B,D), round particles predominated at 1 min, while a combination of particles and elongated nanofibers were observed at 10 min. Likewise, round particles and nanofibers were observed in 10 μM CATCH(+/-) samples at 4°C (Fig. S7C,E,F), with heterogeneity observed in experimental replicates (Fig. S8). No structures were observed in 1x PBS, CATCH(+), or CATCH(-) samples maintained at 4 °C (Fig. S9). Collectively, these observations suggested that decreasing temperature may slow the co-assembly process or bias CATCH peptides toward oligomerization, depending on whether oligomer formation is on- or off-pathway.

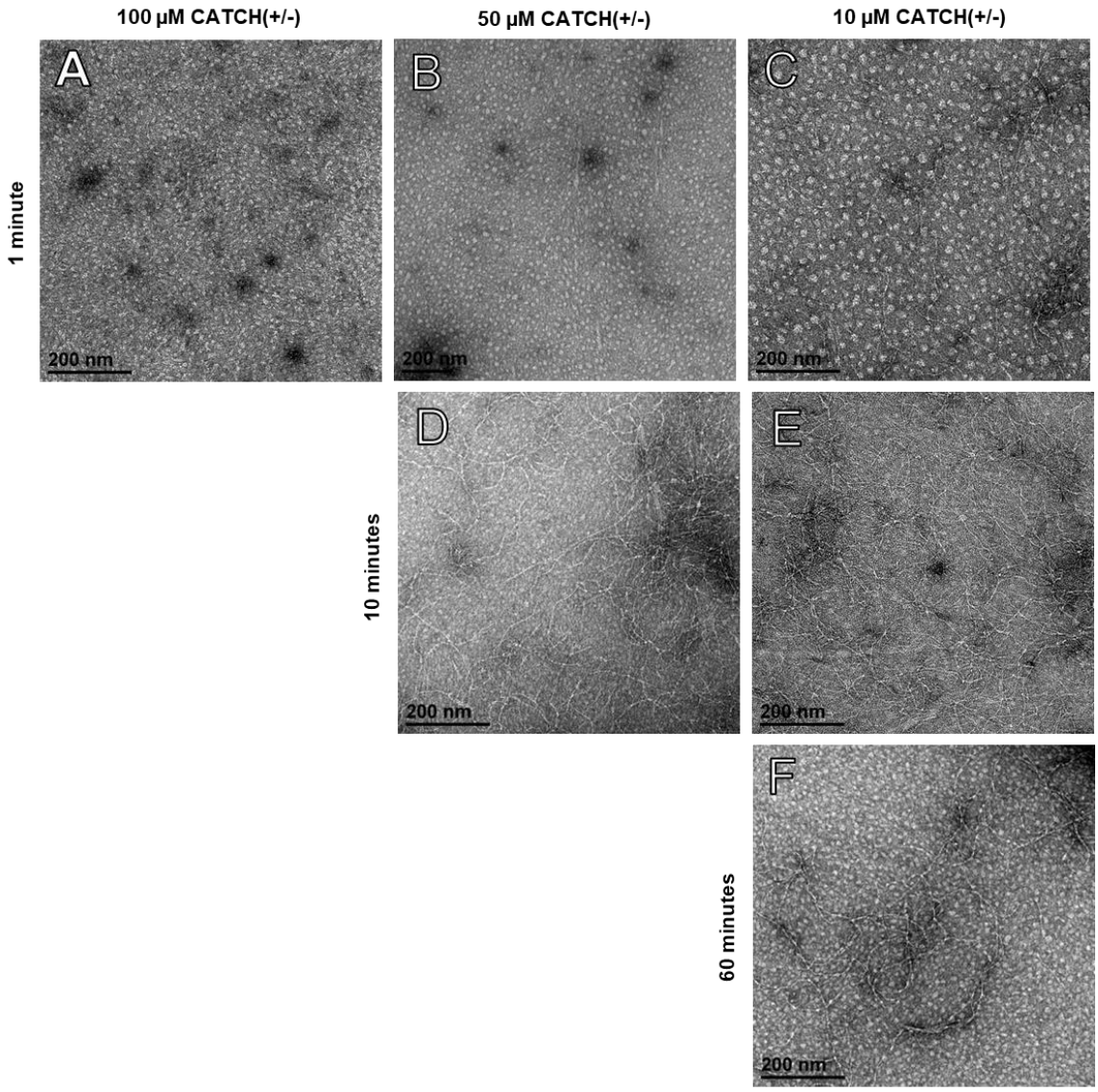

Fig. S7. Full-size electron micrographs of 100 (left column), 50 (center column), and 10 μM (right column) CATCH(+/-) at 1 min (top row), 10 minutes, (middle row), and 60 minutes (bottom row) prepared at 4 °C.

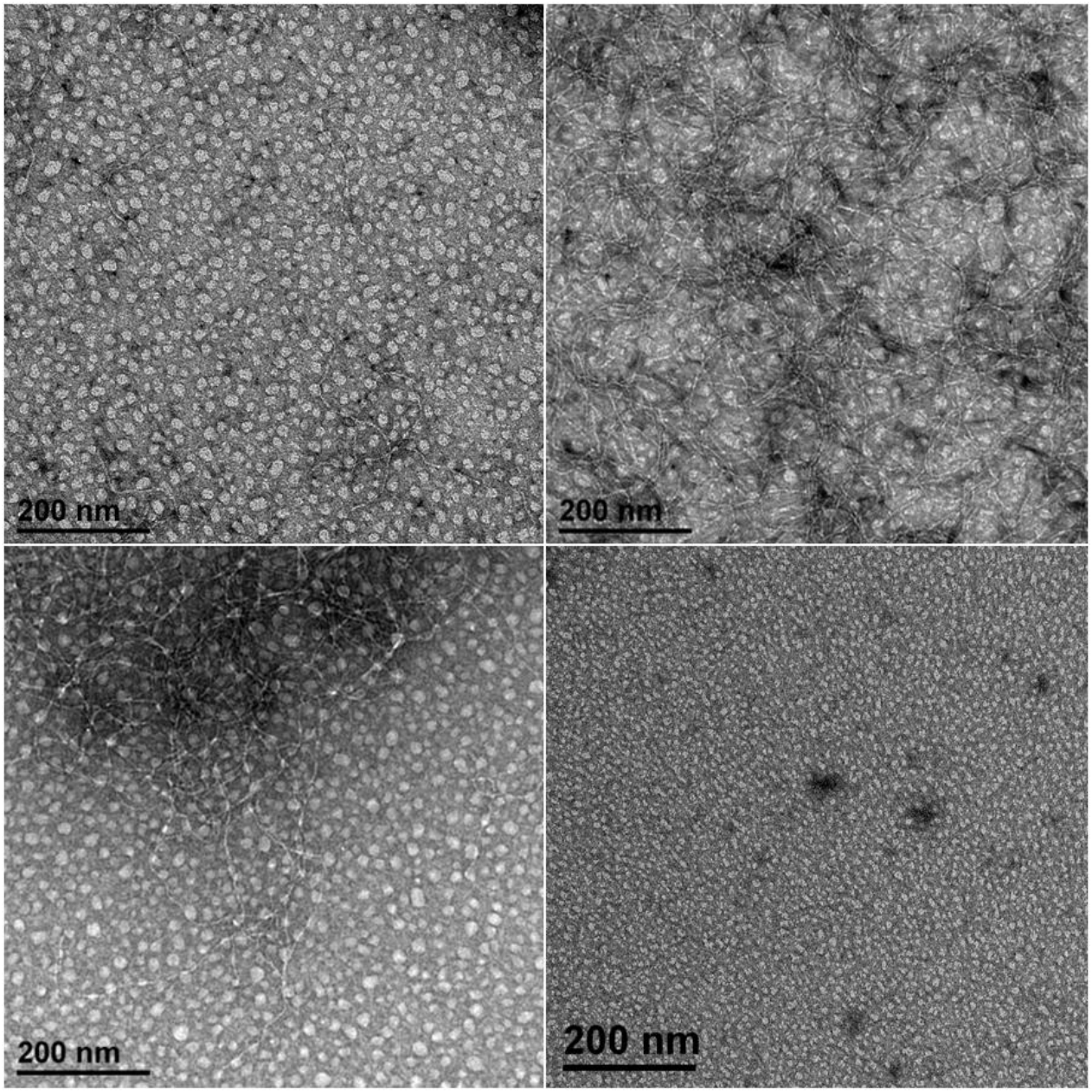

Fig. S8. Full-size electron micrographs of 10 μM CATCH(+/-) at 4 °C and 1 min demonstrating sample heterogeneity.

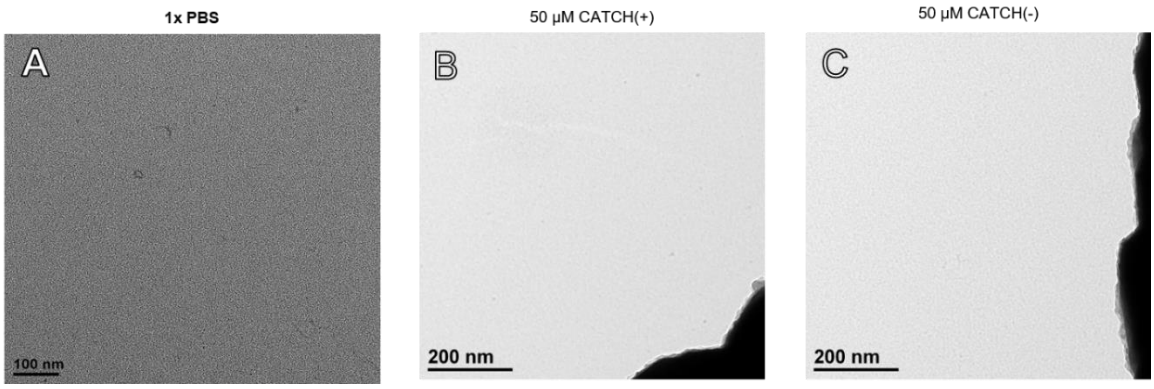

Fig. S9. Electron micrographs of (A) 1x PBS, (B) 50 µM CATCH(+), and (C) CATCH(-) prepared at 4 °C.

Dynamic Light Scattering

We noted some variability in TEM images collected from replicates of equimolar CATCH(+/-) mixtures, particularly at 10 μM (Fig. S8), with regard to the formation of oligomers versus nanofibers. To account for the possibility that TEM sample drying could alter co-assembly structure, mixtures of different concentrations of CATCH(+/-) were analyzed in aqueous conditions using dynamic light scattering at 1 min and 60 min at room temperature (Fig. 4D and Fig. S10A,B). 100 μM CATCH(+/-) samples had large structures with hydrodynamic diameters in excess of 1000 nm at all time points, which corroborated TEM images suggesting that elongated nanofibers were the prevalent species in these samples (Fig. 4D, left). Large structures predominated in 50 μM CATCH(+/-) samples at both time points, although smaller structures of ~100-200 nm were also detected (Fig. S10B). 10 μM CATCH(+/-) samples were predominated by small structures at both 1 and 60 min (Fig. 4D, right), although some variability was noted in independent replicates analyzed at 1 min (Fig. S10C). Notably, the hydrodynamic diameters of structures detected by DLS in most 10 μM CATCH(+/-) samples were comparable to those of the non-fibrillar oligomers observed with TEM, suggesting that sample drying did not appreciably alter oligomer hydrodynamic size. No structures could be accurately detected in samples of either CATCH peptide alone (Fig. S10D).

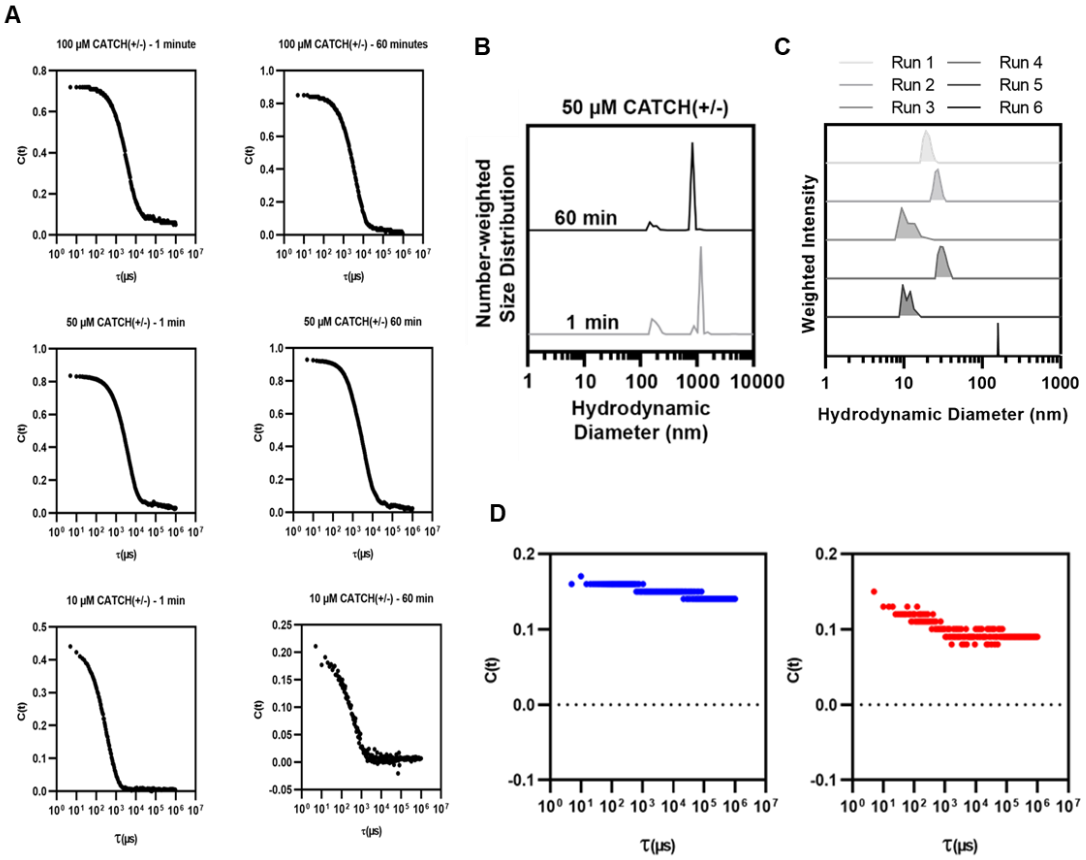

Fig. S10. (A) DLS correlation coefficients from measurements shown in Fig. 4D and Fig. S10B. (B) DLS of 50 μM CATCH(+/-) at 1 and 60 minutes. (C) Independent replicates of DLS measurements of 10 μM CATCH(+/-) incubated for 1 minute demonstrating variability in hydrodynamic size. (D) DLS measurements of CATCH(+) and CATCH(-) alone at 10 μM. The poor fit of the correlation function (bottom row) suggests that no real structures are present over the range of 2-2000 nm.

Simulating effects of AA and BB nearest neighbors on PITHIRDS-CT measurements

The PITHIRDS-CT measurements on "isotopically diluted" CATCH(+/-) nanofibers in the presence of varying probabilities of CATCH(+):CATCH(+) and CATCH(-):CATCH(-) nearest neighbors was modeled using a combination of Monte Carlo simulations of co-assembled β-sheet arrangements with nuclear spin simulations. Figure S11 illustrates the workflow used to generate predictions of PITHIRDS-CT decay curves for a given self-association probability. In this model, we assume an ideal antiparallel β-sheet structure. As shown in Figure S12, an ideal antiparallel β-sheet fits the "isotopically pure" CATCH(+/-) nanofiber sample better than an ideal parallel β-sheet. Simulations of PITHIRDS-CT measurements do not vary significantly up to 30 ms of ^{13}C-^{13}C recoupling time (Fig. 12A-B). Therefore, we determine the probability of AA or BB pairs by evaluating the earlier ^{13}C signal decays using a linear fit of the two extreme cases, p =1 (self-sorting) and p=0 (ideal co-assembled).

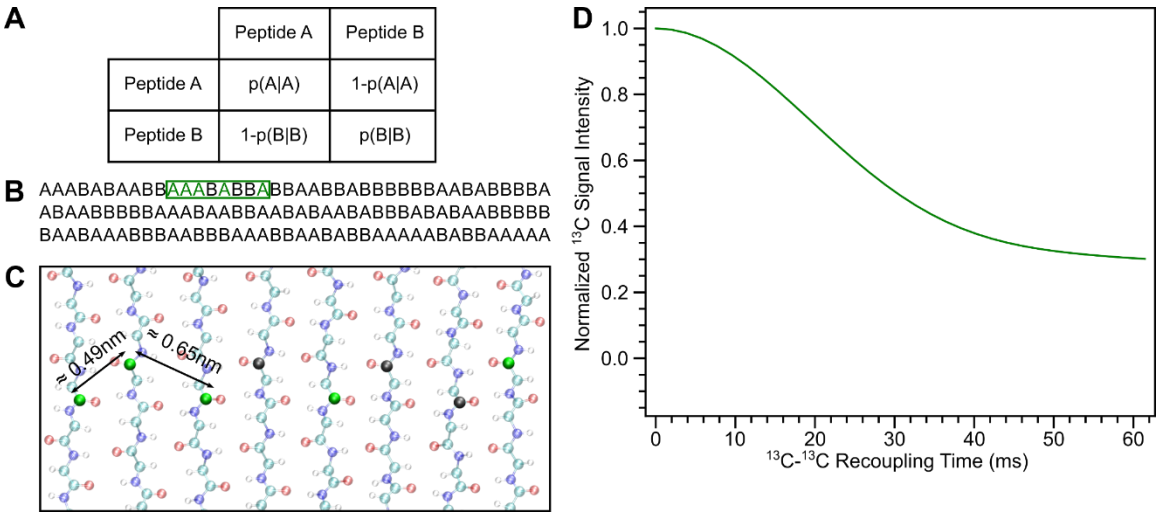

Fig. S11. Calculation of a PITHIRDS-CT decay curve from a Monte Carlo simulation. A) Probability matrix for the Monte Carlo simulations of co-assembled β-sheets, where p(A|A) indicates the probability of adding peptide A to the β-sheet end given A. B) An example sequence produced from a Monte Carlo simulation at a self-association probability of 50%. The green box indicates an 8-molecule sampled segment where isotopically labeled ^{13}C sites (peptide A) are highlighted by green letters. C) Space-filling model of the peptide backbones for an ideal 8-molecule antiparallel β-sheet. Green spheres indicate ^{13}C sites (peptide A) while gray spheres represent unlabeled ^{12}C sites (peptide B) according to the pattern highlighted in panel A. D) Simulated PITHIRDS-CT decay curve of the ^{13}C-spin arrangement depicted in panel B.

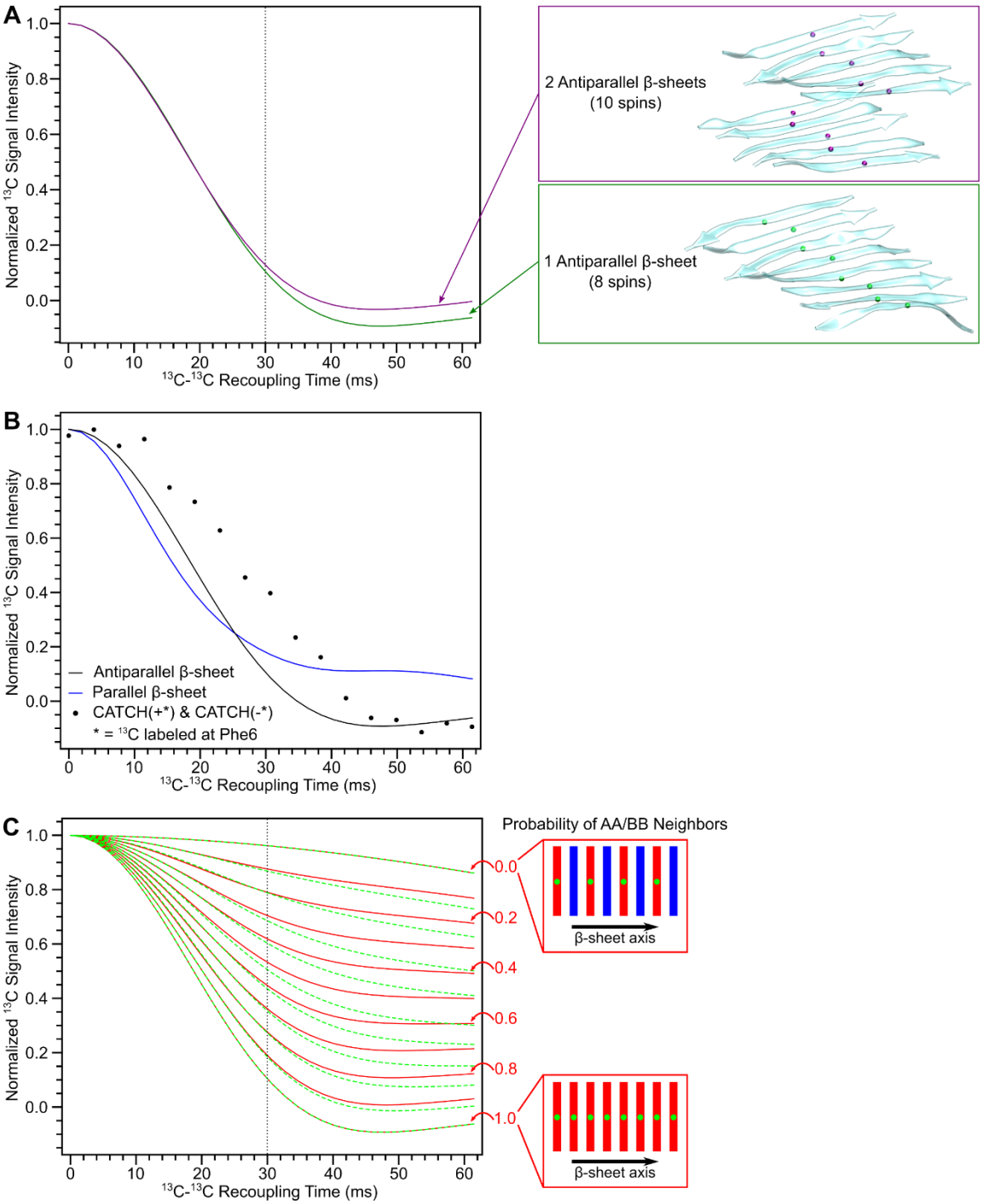

Fig. S12. Effects of different β-sheet models on simulated PITHIRDS-CT decay curves. A) Comparison of simulated PITHIRDS-CT decay curves for a single antiparallel β-sheet (solid green) and two stacked antiparallel β-sheets (solid purple). B) Comparison of experimental PITHIRDS-CT measurement on an "isotopically pure" sample (black dots) against simulated PITHIRDS-CT decay curves for an ideal parallel β-sheet (solid blue) and an ideal antiparallel β-sheet (solid black). C) Comparison of simulated PITHIRDS-CT decay curves determined by Monte Carlo simulations (dashed green) or a linear combination (solid red) of the curves at probabilities of 1.0 and 0.0 assuming an ideal antiparallel β-sheet.

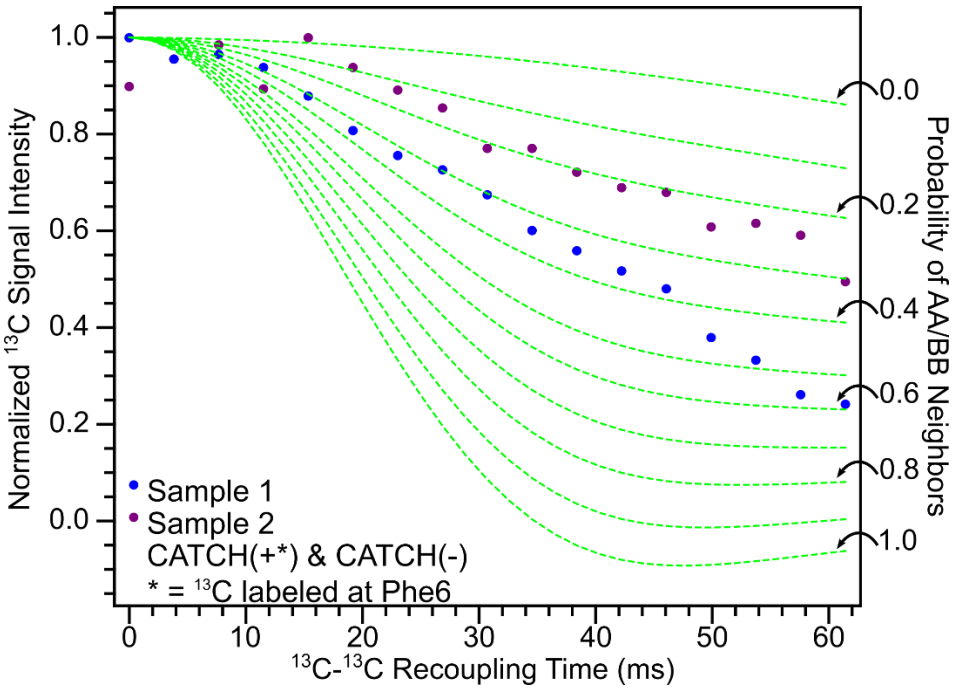

Fig. S13. Comparison of PITHIRDS-CT decays for two different nanofiber samples in which CATCH(+) is isotopically labeled while CATCH(-) remains unlabeled.

Sampling effects on Monte Carlo predictions of β-sheet arrangements

To understand how the number of peptide strands and number of simulations affect the calculated probability of AA or BB nearest neighbors, we ran multiple Monte Carlo simulations of co-assembled β-sheet arrangements at two different self-association probabilities, 0.1 and 0.3. As can be seen in Fig. S14, the calculated self-association probability for a given Monte Carlo simulation run approaches the steady-state probability, depicted as a dashed line, only after thousands of β-strands are added. The Monte Carlo simulations show significant variability at 96 β-strands (the system size of the DMD simulations). Sufficient sampling by running multiple simulations and averaging over a series of simulations can reduce variability in the calculation of self-association propensities as shown in Fig. S15. Hundreds of simulations are needed to reduce sampling variability and approach the true steady-state probability. The size of simulation and number of simulation runs necessary to accurately predict self-association probabilities from DMD simulations would be too computationally costly.

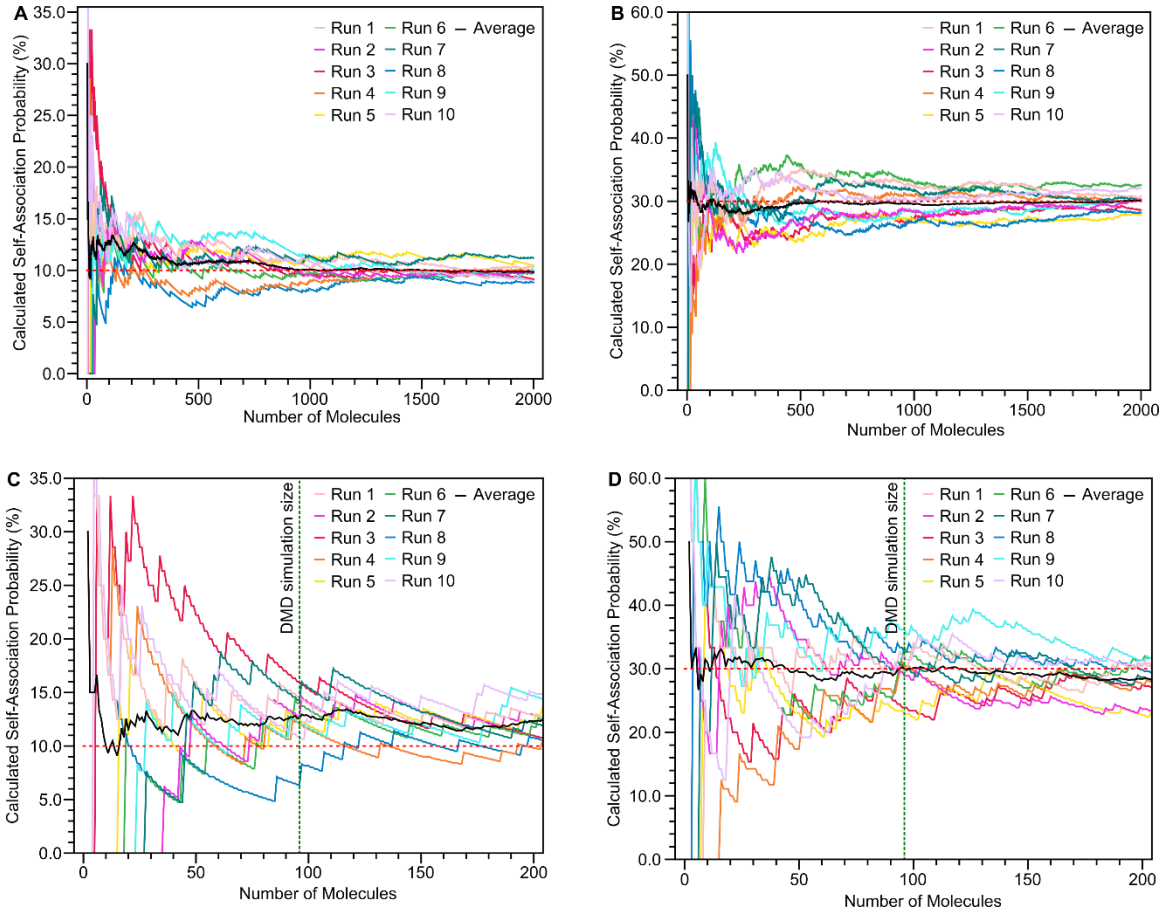

Fig. S14. System size effects on calculated self-association probability from Monte Carlo simulations of co-assembled β-sheets. A) Self-association probability set to 10%. B) Self-association probability set to 30%. C) Close-up of panel A. D) Close-up of panel B.

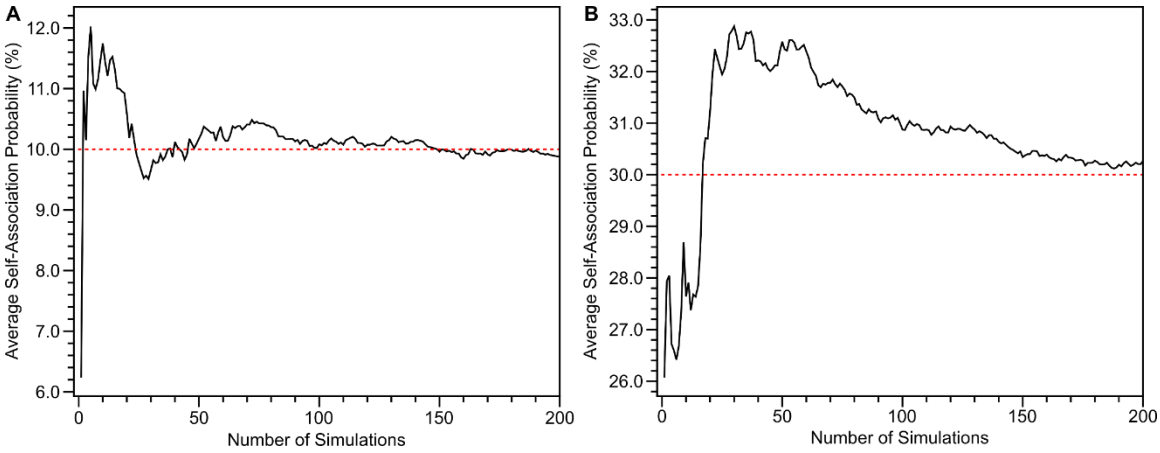

Fig. S15. Effect of simulation runs on the calculated average self-association probability for Monte Carlo simulations of co-assembled β-sheets consisting of 96 β-strands. A) Self-association probability set to 10%. B) Self-association probability set to 30%.

Dehydrated conditions promote CATCH peptide self-assembly

We observed that CATCH(+) and CATCH(-) self-associate into β-sheet structures when dehydrated, which contrasts with their resistance to aggregation in aqueous conditions. FTIR spectra of CATCH(+) and of CATCH(-) peptides individually lyophilized from water have strong maxima near 1620 cm^{-1} (Fig. S16A, B), indicating that the peptides are in a β-sheet conformation when dehydrated. Likewise, PITHIRDS-CT spectra of either lyophilized ^{13}C-labeled CATCH(+) or lyophilized ^{13}C-labeled CATCH(-) have strong signal decays (Fig. S16C), indicating strong dipolar coupling between ^{13}C labeled sites. Such decays would only occur if ^{13}C labeled sites were within ~0.5 nm of each other, consistent with peptides assembled in a β-sheet structure. Collectively, these observations demonstrate that CATCH peptides can self-associate when water is depleted from the system, which may help to explain the formation of AA and BB neighbors in CATCH β-sheet co-assemblies.

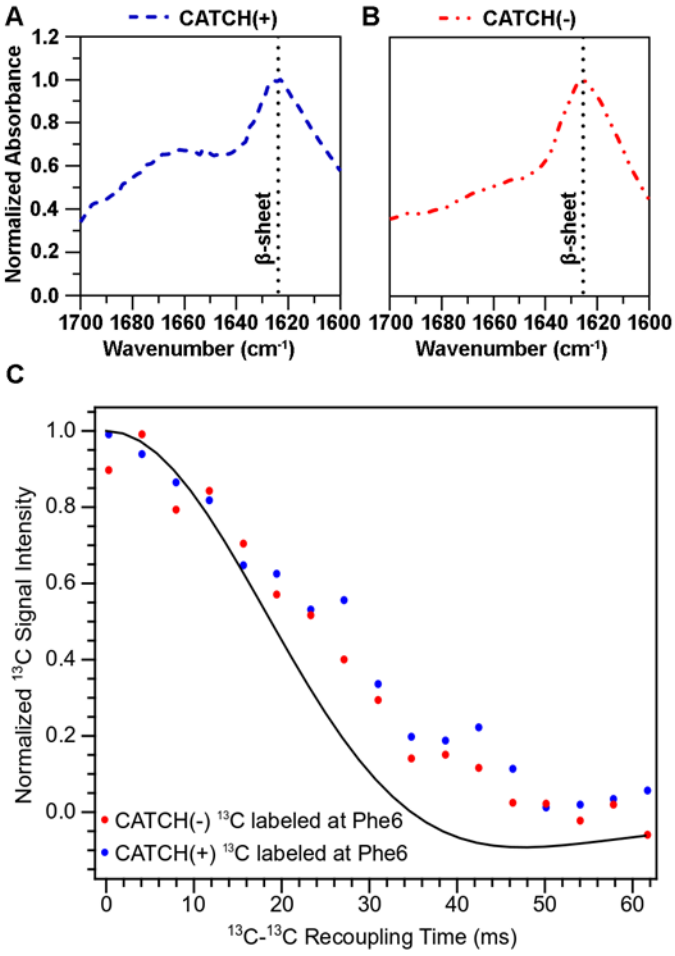

Fig. S16. (A,B) FTIR spectra of CATCH(+) and CATCH(-) lyophilized (C) PITHIRDS-CT measurements of unassembled CATCH(+) and CATCH(-) peptides lyophilized. The solid black curve corresponds to the predicted signal decay in the PITHIRDS-CT experiment from a nuclear spin simulation of eight ^{13}C atoms along an ideal self-assembled antiparallel β-sheet.

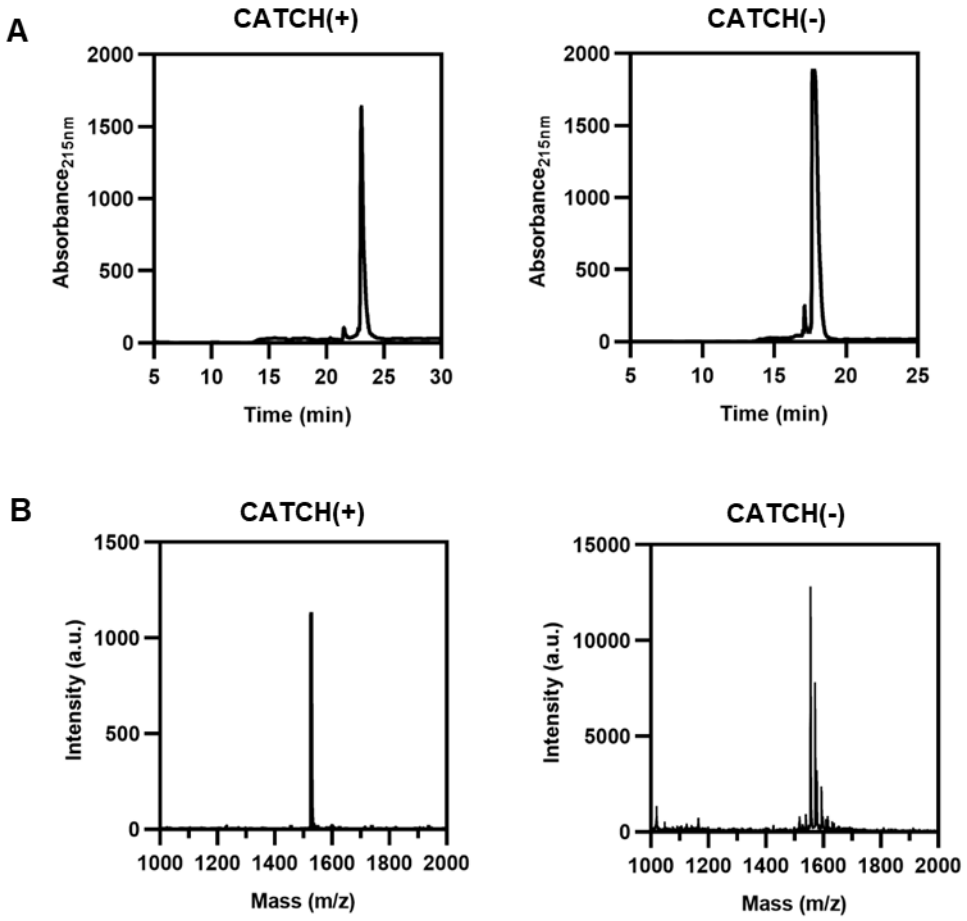

Fig. S17. (A) HPLC traces of ^{13}C labeled CATCH(+) (left) and CATCH(-) (right). (B) MALDI-TOF spectra of ^{13}C-labeled CATCH(+) (left) and CATCH(-) (right).

SI References

1. M. Cheon, I. Chang, C. K. Hall, Extending the PRIME model for protein aggregation to all 20 amino acids. *Proteins: Struct, Funct, Bioinf* **78**, 2950-2960 (2010).
2. A. V. Smith, C. K. Hall, alpha-helix formation: Discontinuous molecular dynamics on an intermediate-resolution protein model. *Proteins: Struct, Funct, Genet* **44**, 344-360 (2001).
3. H. D. Nguyen, C. K. Hall, Spontaneous fibril formation by polyalanines; Discontinuous molecular dynamics simulations. *J Amer Chem Soc* **128**, 1890-1901 (2006).
4. M. Cheon, I. Chang, C. K. Hall, Extending the PRIME model for protein aggregation to all 20 amino acids. *Proteins: Struct, Funct, Bioinf* **78**, 2950-2960 (2010).
5. M. Cheon, I. Chang, C. K. Hall, Spontaneous Formation of Twisted A beta(16-22) Fibrils in Large-Scale Molecular-Dynamics Simulations. *Biophys J* **101**, 2493-2501 (2011).
6. V. A. Wagoner, M. Cheon, I. Chang, C. K. Hall, Computer simulation study of amyloid fibril formation by palindromic sequences in prion peptides. *Proteins: Struct Funct Bioinf* **79**, 2132-2145 (2011).
7. M. L. de la Paz, L. Serrano, Sequence determinants of amyloid fibril formation. *Proc Natl Acad Sci USA* **101**, 87-92 (2004).
8. V. A. Wagoner, M. Cheon, I. Chang, C. K. Hall, Fibrillization Propensity for Short Designed Hexapeptides Predicted by Computer Simulation. *J Mol Biol* **416**, 598-609 (2012).
9. M. Cheon, I. Chang, C. K. Hall, Influence of temperature on formation of perfect tau fragment fibrils using PRIME20/DMD simulations. *Protein Sci* **21**, 1514-1527 (2012).
10. Y. Wang, D. C. Latshaw, C. K. Hall, Aggregation of Aβ(17–36) in the Presence of Naturally Occurring Phenolic Inhibitors Using Coarse-Grained Simulations. *J Mol Biol* **429**, 3893-3908 (2017).
11. M. Cheon, C. K. Hall, I. Chang, Structural Conversion of A beta(17-42) Peptides from Disordered Oligomers to U-Shape Protofilaments via Multiple Kinetic Pathways. *PLoS Comput Biol* **11**, e1004258 (2015).
12. S. J. Bunce *et al.*, Molecular insights into the surface-catalyzed secondary nucleation of amyloid-β_{40} ($A\beta_{40}$) by the peptide fragment $A\beta_{16–22}$. *Sci Adv* **5**, eaav8216 (2019).
13. Y. Wang *et al.*, Simulations and Experiments Delineate Amyloid Fibrilization by Peptides Derived from Glaucoma-Associated Myocilin. *J Phys Chem B* (2018).
14. Y. Wang, Q. Shao, C. K. Hall, N-terminal Prion Protein Peptides (PrP(120–144)) Form Parallel In-register β-Sheets via Multiple Nucleation-dependent Pathways. *J Biol Chem* **291**, 22093-22105 (2016).
15. Y. Wang, C. K. Hall, Seeding and Cross seeding Fibrillation of Prion Protein Peptides PrP(120-144). *Protein Sci* (2018).
16. R. Tycko, Symmetry-based constant-time homonuclear dipolar recoupling in solid state NMR. *J Chem Phys* **126**, 064506-064506 (2007).
17. A. T. Petkova, R. Tycko, Sensitivity enhancement in structural measurements by solid state NMR through pulsed spin locking. *J Magn Reson* **155**, 293-299 (2002).
18. M. Veshtort, R. G. Griffin, SPINEVOLUTION: A powerful tool for the simulation of solid and liquid state NMR experiments. *J Magn Reson* **178**, 248-282 (2006).